Available online at www.sciencedirect.com

SCIENCE DIRECT®

Progress in Solid State Chemistry 34 (2006) 1–20

Progress in Solid State Chemistry

www.elsevier.com/locate/pssc

Electronic process of nitriding: Mechanism and applications

W.T. Zheng [a], Chang Q. Sun [a,b,*]

[a] Department of Materials Science, Jilin University, Changchun 130012, PR China
[b] School of Electrical and Electronic Engineering, Nanyang Technological University, Singapore 639798, Singapore

Received 11 November 2005; received in revised form 11 December 2005; accepted 19 December 2005

Abstract

This article presents consistent insight into the mechanism behind the unusual behavior of nitride compounds in mechanical strength, chemical stability, electron and photon emission ability, and magnetic modulation ability from the perspective of tetrahedron bond formation and its consequence on valence states. In the process of nitridation, a nitrogen atom forms a quasi-tetrahedron with surrounding host atoms through bonding and nonbonding interactions associated with the production of electronic holes and antibonding dipoles. These events add corresponding features of density of states (bonding electrons, nonbonding lone pairs, antibonding dipoles, and holes) to the valence band of the host material, as one can readily observe using ultraviolet photoelectron spectroscopy. It is suggested that the lone pair interactions not only act as the most important function groups in organic molecules but also play important roles in inorganic nitride compounds. The valence alteration, or nitrogen-induced charge polarization and transportation, takes the responsibility for the blue shift in photoluminescence, lowered work function for cold cathode field emission, corrosion and wear resistant, high elasticity for self-lubrication, and magnetic modulation of nitrides as well.
© 2006 Elsevier Ltd. All rights reserved.

Keywords: Nitrides; Bonding; Modeling; Semiconductor compounds; Magnetism; Mechanical strength; Field emission; Photoluminescence

* Corresponding author. School of Electrical and Electronic Engineering, Nanyang Technological University, Nanyang Avenue, Singapore 639798, Singapore. Tel.: +65 6790 4517; fax: +65 6792 0415.

E-mail addresses: wtzheng@jlu.edu.cn (W.T. Zheng), ecqsun@ntu.edu.sg (C.Q. Sun).

URL: www.ntu.edu.sg/home/ecqsun/

0079-6786/$ - see front matter © 2006 Elsevier Ltd. All rights reserved.
doi:10.1016/j.progsolidstchem.2005.12.001

Contents

1. Introduction 2

2. Principle: bond–band–barrier (BBB) correlation 3
   2.1. Nitride tetrahedron formation 3
   2.2. Valence density of states (DOS) 4

3. Verification 5
   3.1. Atomic valence and bond geometry 5
   3.2. Valence DOS formation and lone pair vibration 7

4. Applications 9
   4.1. Corrosion and wear resistivity 9
   4.2. Mechanical strength – harder than diamond? 10
   4.3. Magnetic modulation 12
   4.4. Work function reduction for field emission 13
   4.5. Band-gap expansion for photoemission 16

5. Summary 17

1. Introduction

Nitride compounds have formed a class of materials with fascinating properties that have widely been used for mechanical and elastic enhancement, wear and corrosion resistant, photon and electron emission, as well as magnetic modulation [1]. For instances, investigating the Fe-nitride thin films [2–7] uncovered that the crystal structures, saturation magnetization (M_S) and Curie temperature (T_C) of the FeN films could be modulated by adjusting the concentration of N_2 in the mixture of Ar and N_2 sputtering gases. The M_S value of α''-$Fe_{16}N_2$ phase is ~25% higher than that of the pure Fe (2.22 μ_B). The M_S value drops with increasing N concentration in the films associated with crystal structure transition from ε-, γ-, ξ-, to amorphous phase. Amorphous FeN films exhibit, however, paramagnetic features. An addition of N to the rare earth (R) ferromagnetic (Co and Fe) system increases the M_S value and raises the T_C considerably [8,9]. The M_S of the N–R(Fe, Co) alloys was increased by about 30–40% relative to their parent alloys [9]. The N-modulated M_S may enable these kinds of materials to be used in high-density data storage and in new kinds of strong permanent magnets. Inclusion of N in the synthetic diamond films could significantly reduce the threshold of cold cathode emission of diamond thin films [10]. The threshold field of electron emission of nitrogenated carbon films is even lower than that of carbon films doped with boron and phosphorous. The work function of carbon nitride films deposited at 200 °C substrate temperature under 0.3 Pa nitrogen pressure [11] in sputtering could be reduced to ~0.1 eV. Nitridation can create a band gap and turn a conductor into a semiconductor or even an insulator, such as AlN [12], GaN [13], and InN [14]. N-based group-III and -IV semiconductors are prosperous materials for blue and green light emitting [15]. These wide-band nitride semiconductors have been commercially available for applications in flat-panel displays and blue-ultraviolet laser diodes that promise high-density optical data storage, optic-communication, and high-resolution laser printing. Although experimental indications were

unsatisfactory in the search for a superhard phase of carbon nitride [16–24], the nitride films have shown surprisingly high elasticity (~100%) and high mechanical strength at relatively lower indentation load (<1 mN) [23,25–28].

Even though the performance of nitride compounds has been intensively investigated and widely used, understanding the correlation between the local atomic-bonding, or the energy-band structures, and the observed, or predicted properties of such compounds is still in its infancy [23,25,29]. Concerns about the correlation between the chemical bond and valence density of states and their effects on materials performance are therefore necessary. Deeper and consistent insight into the nitride systems towards predictive design of functional materials would be a challenge. In the present report, we extend the recently developed bond–band–barrier (BBB) correlation mechanism originated for oxidation [30] to the unusual performance of a nitride towards consistent insight into the chemical stability, mechanical strength, magnetic tunability and electronic and optical emission properties.

2. Principle: bond–band–barrier (BBB) correlation

2.1. Nitride tetrahedron formation

Fig. 1a illustrates the physical model of a nitride (NA_4) quasi-tetrahedron obtained by replacing the hydrogen in the NH_3 molecule with atoms of arbitrary element A that should be less electronegative than N. Upon interacting with atoms A in a solid phase, the sp orbital of the N atom hybridizes essentially into four directional orbitals. To fill up the four directional hybridized orbitals of the N atom, three more electrons are required from the A neighbors. Therefore, among the four hybridized orbitals, there are three bonding orbitals occupied by the bonding electron pairs shared by the N and the A atoms and one orbital is occupied by

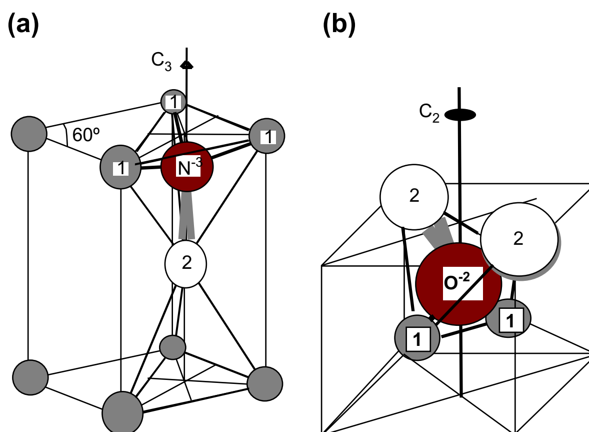

Fig. 1. Primary (a) NA_4 nitride and (b) OA_4 quasi-tetrahedron model [29]. Smaller ions donate electrons to the central N/O acceptor of which the sp orbital hybridizes with production of a nonbonding lone pair. The atoms labeled two are the lone pair-induced A dipole. O/N hybridizes and interacts with arbitrary element A through bonding and nonbonding lone pair to form the quasi-tetrahedron: $NA_4 = N^{3-} + 3A^{+}$ (labeled 1) $+ A^{dipole}$ (labeled 2), and $OA_4 = O^{2-} + 2A^{+}$ (labeled 1) $+ 2A^{dipole}$ (labeled 2). The number and orientation of the lone pair give different geometrical symmetry as indicated.

the nonbonding electron lone pair of the N alone. Because of its higher electronegativity (3.0 without unit), the N atom acts as an electron acceptor rather than a donor and therefore the three bonds are mainly polar-covalent. The nonbonding lone pair formation is an intrinsic property of nitrogen and oxygen upon sp-orbital hybridization, which is independent of whatever the less electronegative constituent A atom is.

However, the lone pair tends to polarize the neighboring atom (dipole formation in Fig. 1) on which the lone pair is acting. Upon the tetrahedron formation, the A atoms surrounding the central N atom will change their valences. The smaller A^+ ions donate electrons to the N acceptor, and the neutral N becomes N^{3-}. The atoms labeled two are the lone pair-induced dipoles, A^{dipole}. As consequences of the tetrahedron formation, the A^+ ions and the A^{dipole} also polarize their neighbors to form antibonding dipole states as well. As noted by Atkins [31], the antibonding states are dominated by the less electronegative elements, and therefore, antibonding interaction forms between the $A^{dipole} \leftrightarrow A^{dipole}$ dipoles rather than between the N^{3-} and the A^+ ions. In a particular nitride system, the geometrical environment determines the orientation of the nitride tetrahedron. The difference between a nitride tetrahedron and an oxide tetrahedron (Fig. 1b) [29] is that one oxide tetrahedron has two lone pairs while the nitride tetrahedron has only one. The number of lone pair in the tetrahedron follows a '4-n' rule, where n is the valence value of the electronegative additive. This premise may be extended to other electronegative elements such as S and F. This difference in the number of lone pair determines that the group symmetry of a nitride tetrahedron differs from that of an oxide tetrahedron. The former prefers a C_{3v} group symmetry and the latter C_{2v}. Such a small difference determines that a nitride performs entirely different from an oxide in many situations. If the N or O acceptor is over dosed, a hydrogen-like bond is formed, which transports electrons from the antibonding states to the bonding orbitals of the acceptors [29]. Unfortunately, the events of nonbonding lone pair and antibonding dipole formation are often oversighted in inorganic chemistry.

2.2. Valence density of states (DOS)

Because of the NA_4 and OA_4 tetrahedron formation, the energy-band of the A host solid is modified with four additional valence DOS features. As illustrated in Fig. 2, the difference in the DOS between a nitride or an oxide compound and its parent A solid leads to the bonding ($<E_F$), nonbonding ($\leq E_F$), holes ($\leq E_F$) and antibonding ($>E_F$) states [29,30]. The positions of the electron holes in energy space are located at the upper edge of the valence band of a semiconductor or below the E_F of a metal. The bonding states are slightly lower while the nonbonding states are around the original p-levels of an isolated N/O atom, as nonbonding states neither add nor decrease the system energy [31]. Electrons of the dipoles occupy the empty states well above E_F as they gain energy upon polarization. The bonding and antibonding processes yield holes under E_F, which turns a metal to be a semiconductor such as group-III nitride/oxide compounds [15]. Due to the hole production, the effective band gap of an intrinsic semiconductor is chemically widened such as the cases of Ge and Si nitride/oxide [32]. The dipole formation enhances the charge density of the surface atomic layers and hence reduces the work function of the system [33]. The alteration in atomic sizes and valences modifies the potential barrier or the morphology of the surface. From this perspective, nitrogen additives not only act as acceptors to produce holes at the valence band edge but also act as donors with additionally localized nonbond and antibond states.

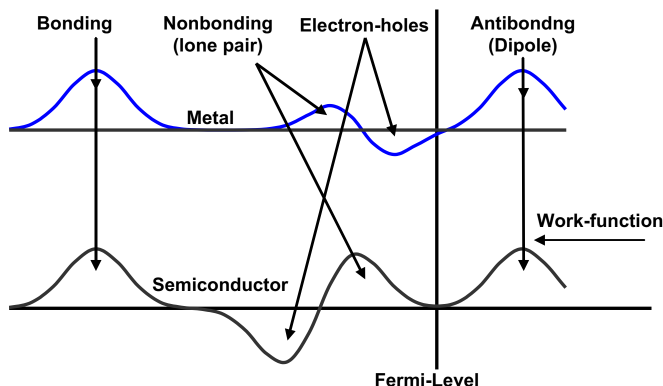

Fig. 2. N and O induced valence DOS differences between nitride/oxide compounds and the parent metal (upper) or the parent semiconductor (lower). The N or O modifies the energy-band of the host by adding four features through the following processes [29]: (i) charge transport from A to the acceptor to form the sp^3-hybrid bonding, which produces states at locations slightly lower than the 2p-level of the acceptor; (ii) the sp^3-hybridization produces nonbonding lone pair states that neither raise nor lower the system energy; (iii) lone pairs and ions induce antibonding dipoles that form states well above the E_F, which lowers the work function; and (iv) formation of bonding and antibonding generates electron hole states close to E_F of a metal or near the valence band edge of a semiconductor, which changes a conductor to be a semiconductor or widens the band gap of a semiconductor; (v) additional acceptor will attract the electrons of the dipoles to form hydrogen-like bond that narrows the antibonding density of states and restores the work function.

3. Verification

3.1. Atomic valence and bond geometry

The C_{3v} symmetry of an NA_4 cluster can be evidenced directly by the fact that most of the nitrides prefer the hcp(0001) or the fcc(111) orientation, such as AlN, GaN, TiN, etc. Fig. 3 shows the scanning electron microscopy images of SiCN crystals grown using microwave-assisted CVD on Si substrate with a gas mixture of $N_2 + CH_4$ [34]. It is apparent that the SiCN crystallites prefer the hcp columnar structures.

N-chemisorption study by Sotto et al. [35] suggested that the Cu_3N forms on the Cu(001) and Cu(h11) surfaces with nitride patches that are imaged with the scanning tunneling microscopy (STM) as being $\sim$0.8 Å below the clean surface. The STM depression often corresponds to ions or atomic vacancy. Low-energy-electron diffraction (LEED) study of the N-Ru(0001) surface [36] reveals that the N atom sinks deeply into the threefold hollow-site of the top layer associated with a radius-away reconstruction of the N-Ru(0001) surface. The radial-away reconstruction indicates a central position of the N in the NRu_4 cluster of C_{3v} symmetry with lone pair directing downward the surface according to the current premise of tetrahedron formation. X-ray-excited Auger electron, electron energy-loss, and ultraviolet photoemission spectroscopic (UPS) investigations of GaN(0001)-(1×1) surface [37] revealed that nitride bond formation proceeds in the same way to the ammonia and aniline formation: the N atom is located in a fourfold-coordinated configuration bridging two surface Ga atoms. However, for the N-Ni(001) surface, the lone pair is directed sideways into the open end of the surface and the electrostatic interaction between the alternative Ni^+ and Ni^{dipole} drives the Ni(001) surface to be reconstructed with rhombi-chain forming along the $\langle 11 \rangle$ directions [38] (see Fig. 4). Compared with C adsorption that produces compressive stress, N addition leads to tensile stress at

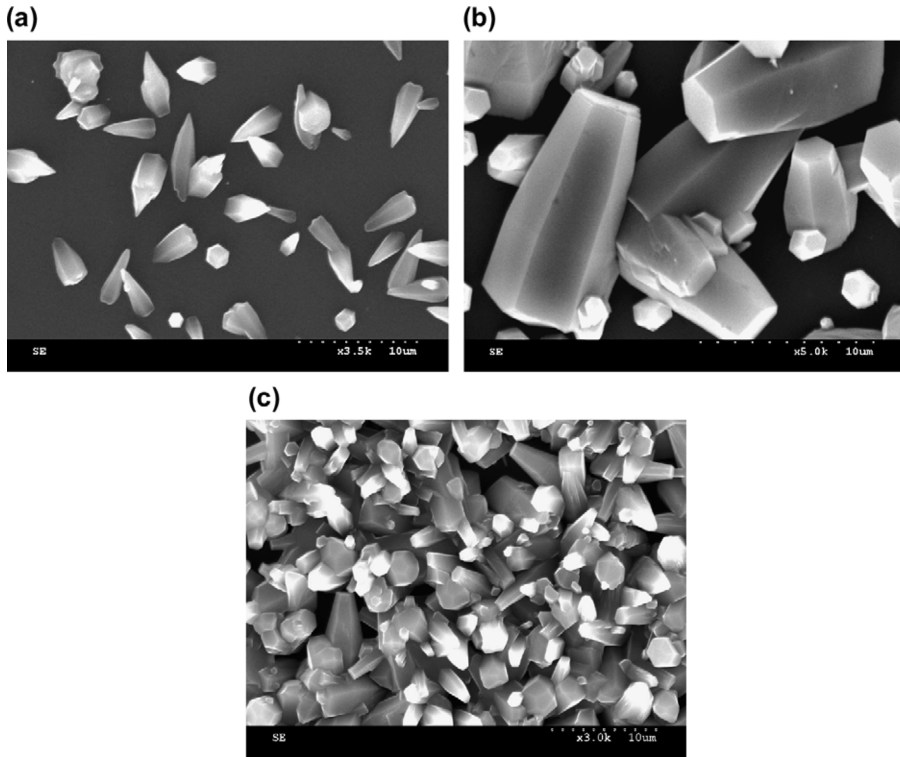

Fig. 3. SEM images of the SiCN crystals formed on Si substrate with a 10/4 sccm N_2/CH_4 gas mixture for (a) 4 h, (b) 10 h, and (c) 50/1 sccm for 10 h. SiCN crystallites prefer the hcp structures [34].

the surface due to the different atomic valences. Understanding of the N and C induced Ni(001) surface reaction provides not only a consistent insight into the mechanism for the clock-and-anticlock wise reconstruction [39] but also a novel approach of TiCN graded buffer layer to neutralize the interfacial bond stress and hence to substantially enhance the diamond–metal adhesion [40].

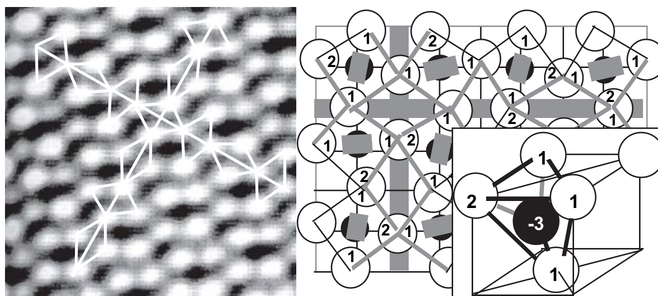

Fig. 4. (a) STM image and (b) the corresponding bond network for N-induced Ni(001) surface reconstruction with rhombus-chain formation along the $\langle 11 \rangle$ direction. The atoms labeled 1 and 2 in the basic tetrahedron represent Ni^{+} and Ni^{dipole} [38]. The depressions link two Ni^{+} at the surface.

3.2. Valence DOS formation and lone pair vibration

Compared with the nanometric SiC, nanostructured SiN has been revealed using X-ray-photoelectron and soft-X-ray spectroscopes two additional DOS features [41]. One is located at ~3.3 eV below E_F and the other is 1–3.8 eV above E_F. The former feature below E_F was identified as the N-2p lone pair π-orbital at the upper edge of the valence band of SiN. The latter unknown feature can readily be ascribed as the contribution from the lone pair-induced antibonding states according to the current BBB correlation. A first-principle calculation [19] predicted that the N–N lone pair repulsion in the carbon nitride leads to a ~2.2 eV elevation in antibonding energy. The ab initio calculations of the N-Ru(0001) surface [36] and O-Ru(10$\bar{1}$0) surface [42] reveal the similar DOS features at +3.0 (antibond), −1.0 (holes), −3.0 (nonbond) and −6.0 eV (bond) around E_F, as compared in Fig. 5, which are consistent surprisingly well with predictions of the current BBB correlation premise (Fig. 2). The energies of the states may vary from specimen to specimen but the number of the DOS features and their relative position should be common for nitride and oxide compounds. Fig. 6 shows the evolution of the valence DOS features upon C being gradually replaced by N in a TiC compound. The shaded broad peak around E_F can be attributed to the lone pair DOS whereas the energy of the antibonding DOS is beyond the scope of normal X-ray photoelectron spectroscopy (XPS), but it is detectable with the inverse ultraviolet photoelectron spectroscopy (IUPS) or scanning tunneling spectroscopy (STS) [30]. STS measurement [43] has revealed strong DOS features in the conduction band of CN_x nanotubes near the Fermi level (−0.18 eV), evidencing the existence of the lone pairs. For carbide, neither lone pair nor antibonding dipole could form upon reaction. However, a ~2.31 eV antibond DOS has been obtained in calculating carbon nitride [19]. Table 1 compares the DOS features of metal and semiconductor nitrides supporting the model predictions. Recent XPS, UPS, near-edge X-ray absorption fine structure spectroscopy (NEXAFS), as well as X-ray emission spectroscopy (XES) measurements of carbon nitride films [44] revealed three significant DOS features that were attributed to the lone pair (~−3.8 eV), σ (~−8.8 eV) and π (~−6.4 eV) bond configurations.

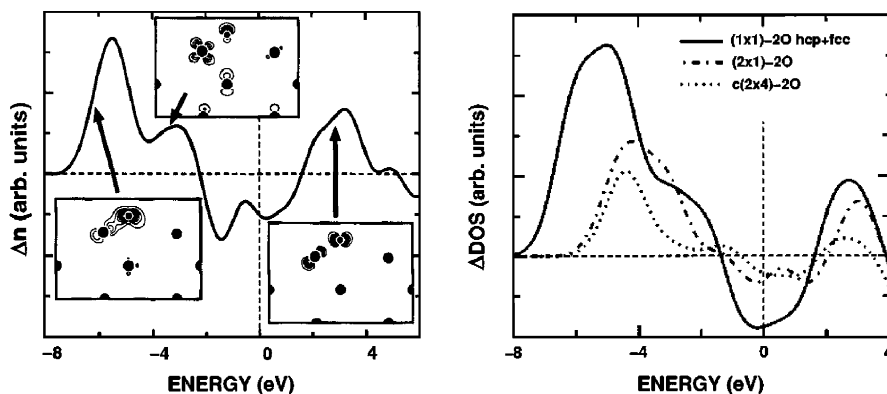

Fig. 5. The tight-binding approximation of the difference in the density of states, n(Ru + N/O) − n(Ru), between Ru(0001)-c(2 × 2)-N, Ru(1010)-c(2 × 1)-O, and Ru(0001) surface suggests four DOS features corresponding to the antibonding (~3.0 eV), hole (−1.0 eV), nonbonding (−3.0 eV) and bonding (−6.0 eV) states [36,42], which concur with the current BBB prediction on O and N addition.

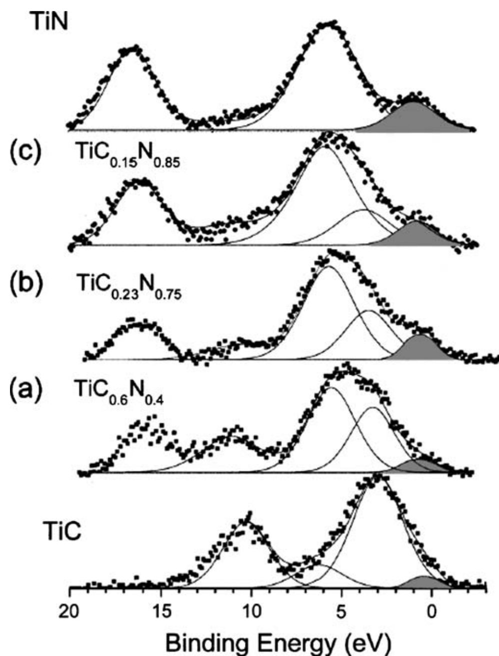

Fig. 6. XPS profiles show the evolution of the valence DOS from TiC to TiN showing the additional shaded features around E_F [50] that can be attributed to the lone pair.

The presence of the lone pair in both oxide and nitride has been further confirmed using the Raman spectroscopy showing vibration features below 1000 cm^{-1} [25,45], as compared in Fig. 7, which is consistent with the frequency of H bond vibration in biomolecules such as protein and DNA [46]. The lone pair interaction might be a key significance in messaging and signaling of biomolecules. Compared with the Raman spectra of nitrides, the lone pair features of oxides are much stronger because the latter has one more lone pair in a tetrahedron compared with the former nitride. It has been shown that [47,48] the lone pair plays significant role in determining the optical properties of carbon nitrides both in the visible and in the infrared (IR) photon energy ranges. In the IR, the extra-electrons related to nitrogen lone pair will affect the medium-range polarization and lead to the sharp vibrational absorption features at 1000–1900 cm^{-1}.

Table 1
N adsorbate-derived DOS features adding to the valence band of metals (unit in eV)

N-added surfaces	Antibond (dipole) $> E_F$	Nonbond (lone pair) $< E_F$	Bond (sharing pair) $< E_F$
N-Cu(001) [49]	3.0	−1.2	−5.6
N-Ru(0001) [36]	3.0	−3.0	−6.0
TiCN [50]	0.0 ± 1.0		−5.7
a-CN [51]		−4.5	−7.1
CN [52]		−2.3	
N-Ag(111) [53]		−3.4	−8.0

Holes are produced below E_F. All the data were probed with XPS unless otherwise indicated.

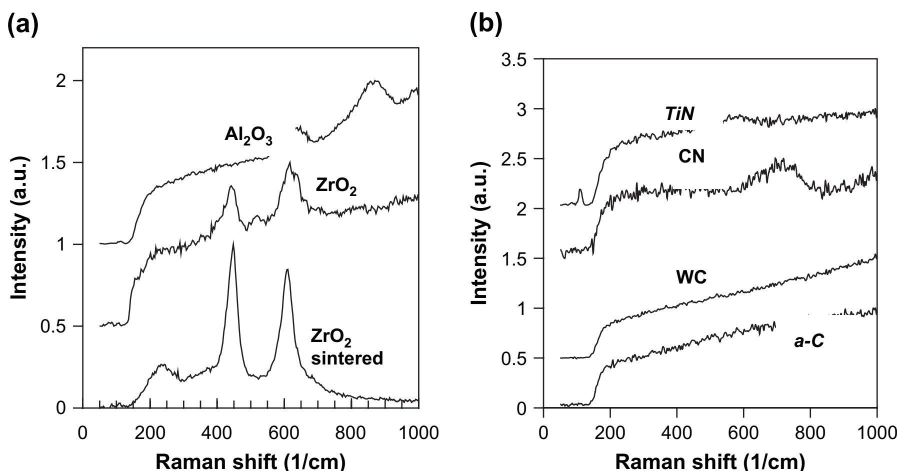

Fig. 7. Low-frequency Raman shifts indicate the presence of weak bond interaction in (a) Zr (powder and sintered) and Al oxides and (b) Ti and amorphous carbon nitrides. The peaks correspond to the nonbonding electron lone pairs generated during the sp-orbital hybridization. The number of lone pairs follows a "4-n" rule, where n is the valence value of the electronegative additives. For oxides, nitrides and carbides, $n = 2$, 3 and 4, respectively. Therefore, the peak intensities of oxides are stronger than that of nitrides but there are no such peaks at all for amorphous carbon and tungsten carbide [25].

4. Applications

4.1. Corrosion and wear resistivity

We may consider the case that the N reacts with atoms in a surface of C_{3v} symmetry, such as fcc(111) and hcp(0001) planes (for Fig. 1a example). The N atom is located in between the top two layers and the lone pair is directed into the substrate. The surface is hence networked with the smaller A^+ and the saturate bonded N^{3-} ion cores with densely packed electrons. The outer shells of the A^+ ions are emptied due to charge transport from upper DOS states of the host to the lower empty DOS states of nitrogen upon bond formation. The reaction not only lowers but also causes densification of the valence DOS due to the A^+ and N^{3-} formation. Therefore, the top surface layer should be inert in chemistry as it is harder for one additional acceptor to catch electrons from the lowered and densified DOS. Electrons in the saturated bond should be more stable compared with the otherwise unbonded electrons in the neutral host atoms. This configuration may explain why a nitride surface is corrosion resistant.

The high intra-surface strength due to the ionic network could be responsible for the hardness of the top layer. On the other hand, the N^{3-}–A^+ network at the surface is connected to the substrate mainly through the nonbonding lone pair states. The nonbonding interaction is rather weak ($\sim$0.05 eV per bond) compared with the original metallic bonds ($\sim$1.0 eV per bond) or the intra-surface ionic bond (2–3 eV per bond). The weak interaction due to lone pair formation should be highly elastic within a certain range of mechanical loading, which makes the two adjacent surface layers more elastic at a pressing load lower than a critical value at which the weak interaction will break. Therefore, the enhanced intra-layer strength makes a nitride usually harder ($\sim$20 GPa), and the weakened interlayer bonding makes the nitride highly elastic and self-lubricant. Nanoindentation profiles from TiCrN surface and sliding friction measurements from CN and TiN surfaces have confirmed the predicted high elasticity and

high hardness at lower pressing load and the existence of the critical scratching load [25]. As compared in Fig. 8 (a) and (b), under 0.7 mN load of indentation, the elastic recovery and hardness for a GaAlN film [28] are higher than that of an amorphous carbon film. The GaAlN surface is also much harder than the amorphous-C film under the lower indentation load. Fig. 8(c) and (d) shows the profiles of pin-on-disk sliding friction test, which revealed the abrupt increase in the friction coefficient of nitride films under higher load [25]. For polycrystalline diamond thin films, no such abruption in friction coefficient is observed though the friction coefficient is generally higher than the nitride films before bond breaking. The absence of lone pairs in a-C film makes the film less elastic than a nitride film under the same pressing load. The abrupt change in the friction coefficient evidences the existence of critical load that breaks the nitride interlayer bonding – lone pair interaction. Under higher pressing load (5 mN) of indentation, the elastic recovery reaches the values of 65 and 85%, for CN and TiN, respectively [23]. Therefore, the nonbonding interlayer interaction enhances the elasticity of nitride surfaces at pressing load under the critical values. Such high elasticity and high hardness by nature furnish the nitride surfaces with self-lubricate for nano-tribological applications.

4.2. Mechanical strength – harder than diamond?

The search for an exceptionally hard material of C-nitride has lasted for more than one decade. The hardness and the elastic modulus of β-C_3N_4 are predicted to be comparable to or exceeding those of diamond. However, experimental data have shown that no satisfactory though tremendous efforts have been made [54–56]. Only one report showed the success of preparing α-C_3N_4 and β-C_3N_4 powders using the liquid–solid reaction between anhydrous $C_3N_3Cl_3$ and Li_3N in benzene at 355 °C and 5–6 MPa for 12 h [57]. However, the N/C atomic ratio is measured to be about 0.66, much lower than the predicted stoichiometry of 4/3. Theoreticians [18–21] modified the original C–N covalent-bond iteration, indicating that the superhard C_3N_4 phase can only be produced at higher pressure (68 GPa). Considering the nonbonded N–N repulsion, the hypothetic C_3N_4 stoichiometric ratio has to be ruled out, and the N concentration should be no more than 50% [18,19], unless carbon vacancies are presented. If sp-hybridization occurs in both C and N, the ideally allowed N/C ratio is unity.

Actually, experiment results revealed that the hardness of CN films decreases with increasing N content. For instance, the elasticity of the CN has been measured to vary with substrate temperature and the N content. Increasing the substrate temperature from 100 to 350 °C at 2.5 mTorr N_2 pressure, the elastic recovery increases from ~60 to ~90% [25]. At a substrate temperature of 350 °C, increasing N_2 pressure from 2.5 to 10 mTorr could reduce the elasticity to 68% [27]. Although the hardness of CN available to date [23] (~60 GPa) is below that of a diamond (~100 GPa), the elasticity has been confirmed rather high with a critical load for plastic deformation. Agreement between predictions and observations supports the current BBB correlation and the nonbonding repulsion mechanism [16,19]. Therefore, the presence of the lone pair, or the fifth electron in nitrogen, prohibits the carbon nitride from being harder than a diamond.

However, it might be possible to obtain the superhard phase by removing the fifth electron of the N atom in synthesizing the CN crystal under abnormal conditions such as extremely high pressure or high temperature as suggested in Refs. [18–21]. The hardness of nanocrystalline/amorphous composites such as nc-TiN/a-Si_3N_4, nc-TiN/a-Si_3N_4, nc-$TiSi_2$, nc-$(Ti_{1-x}Al_x)N$/a-Si_3N_4, nc-TiN/TiB_2, and nc-TiN/BN could approach that of diamond because of the interfacial mixing effect [58–60]. It has been found that the hardness and elasticity of nanometric

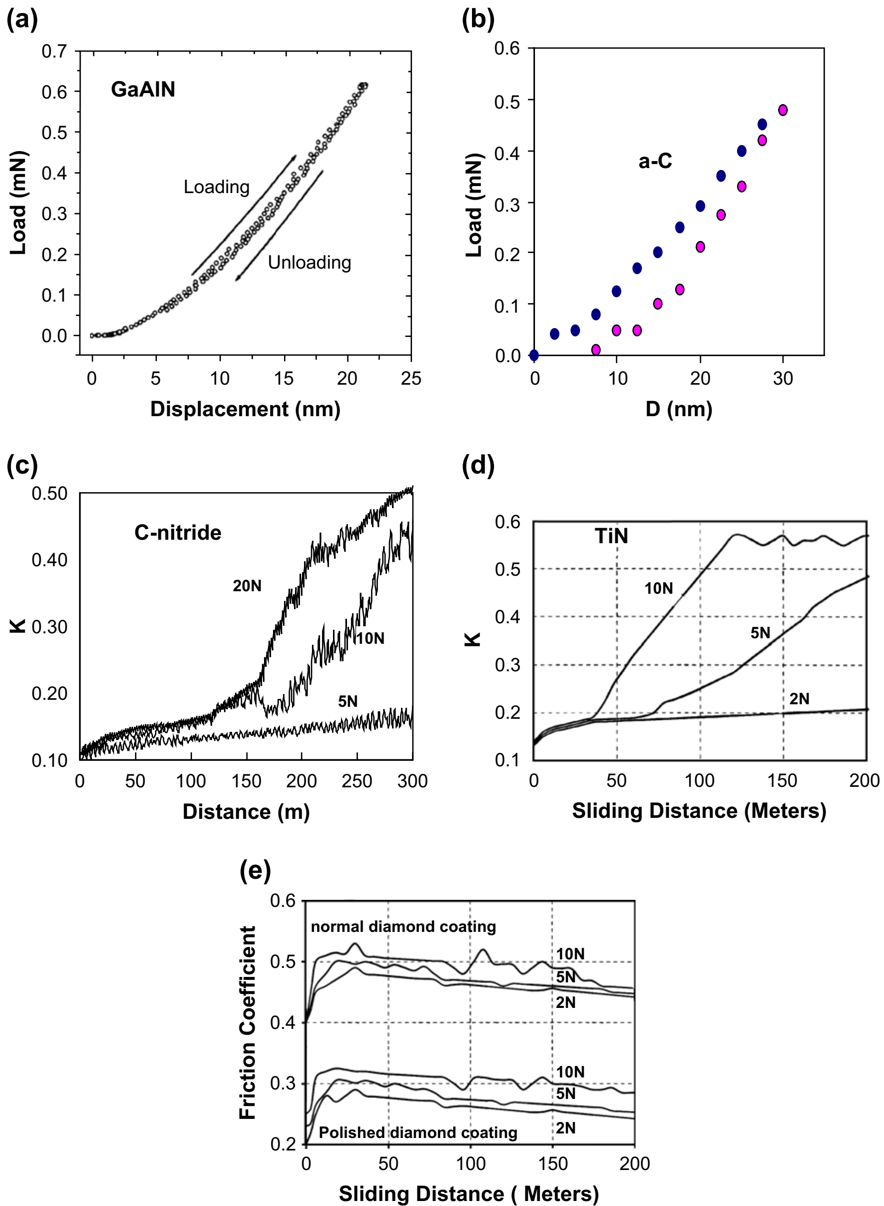

Fig. 8. Mechanical strength and elasticity of nitride films. Comparison of (a) the 100% elastic recovery of GaAlN/Al_2O_3 surface obtained at 0.7 mN load and (b) the 65% elastic recovery of amorphous carbon in the same scale of indentation load. Pin-on-disk measurement of sliding friction shows the abrupt increase in the friction coefficient for (c) C-nitride and (d) Ti-nitride [25] and evidences the critical load that breaks the surface bond. (e) The friction coefficient of diamond thin films shows no abruption features though the coefficient is generally higher than the carbides.

TiN/CrN and TiN/NbN multi-layered thin films increase with reducing structural wavelength (optimal at 7.0 nm) [61,62].

4.3. Magnetic modulation

The α''-$Fe_{16}N_2$ phase firstly discovered by Jack [2,3] is an intermediate in the decomposition of N-martensite Fe_4N. The Fe atoms are displaced from sites occupied in the ferrite lattice by the presence of N atoms which occupy 1/24 the number of octahedral interstices in a completely ordered manner. Up to 1/2 the number of N-atom sites may be vacant. The α''-$Fe_{16}N_2$ phase with N concentration of 5–7 at% shows soft magnetic properties [63] with various magnetization depending on preparation conditions. Single-crystal α'' films prepared by MBE are claimed to have a magnetization of 3.2 μ_B per Fe atom – higher than any other binary alloys. A comparison of the magnetic behavior of equivalent α'-Fe_8N in chemical composition with the α''-$Fe_{16}N_2$ suggested that the magnetic variability is due to different degrees of structural order–disorder because the latter is with a higher N-atom ordering [3].

Fig. 9 shows the N content dependence of the M_S of Fe films deposited using vacuum arc technique [64]. The trend agrees with that measured from FeN films deposited using facing target sputtering method [2].

According to the Ising approximation, the overall M_S under zero external-field is determined by:

$$H_{\text{exchange}} = \sum_{\langle i,j \rangle} J_{ij} S_i \cdot S_j \propto \frac{S_i S_j}{r_{ij}} \cos\theta_{ij} \tag{1}$$

S_i and S_j are the magnetic momentums of individual atom and the J_{ij} is the coefficient of exchange interaction between momentums i and j. θ_{ij} represents the angle between the S_i and S_j moment. There are several factors controlling the H_{exchange} and hence the overall magnetization. θ_{ij} varies with the applied magnetic field; the J_{ij} varies with atomic distance; and S_i and S_j vary with atomic valences. Chemical reaction not only changes the separation between the atoms and hence the

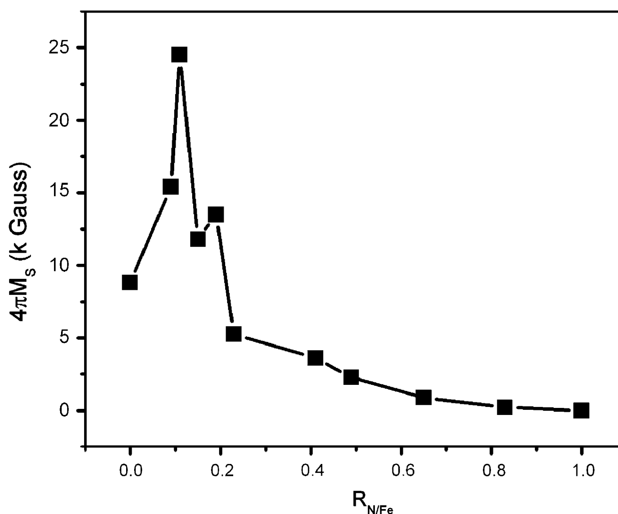

Fig. 9. Nitrogen content dependence of saturation magnetization $4\pi M_S$ of the FeN films [64].

structure ordering [2,3] but also the electron distribution in the orbitals that modify the atomic valence and hence the S_i and S_j values. If the separation is too large, the system will be paramagnetic disregarding the S_i and S_j values. Interatomic distance not only varies with the extent of reaction but also changes as a function of atomic coordination [65]. Here we may focus on the N-modified S_i and S_j values of a Fe-nitride, as a sample. It can be seen from Table 2 that the total angular momentum increases when the Fe alters its atomic valence to Fe^{n+} (n is an integer) or Fe^{dipole}. In the former, the Fe donates 3d electrons to the N acceptor; in the latter, the Fe 3d electrons are propelled by the Coulomb potential of the lone pair and move to an outer shell orbital of the Fe atom, 4p or 4d. The N^{3-} and its electrons do not contribute to the magnetization. The total momentum of the Fe^{n+} varies from 2.0 to 3.0 μ_B and then drops to 2.0 μ_B when the valence is changed from 1 to 4. The momentum for Fe^{dipole} is 4.0 ($3d^5 4s^2 4p^1$) or even 5.0 μ_B ($3d^5 4s^2 4d^1$). The average momentum of an isolated tetrahedron ($N^{3-} + 3Fe^+ + Fe^{dipole}$) is then 2.875 or 3.125 μ_B, being 25–40% higher than that of a pure Fe atom (2.22 μ_B as measured). As discussed, H-like bond formation will lead to $Fe^{+/dipole}$ formation with substantially lowered magnetization. This configuration may explain why the $Fe_{16}N_2$ possesses the higher magnetization compared with Fe_4N phase in which the $Fe^{+/dipole}$ is not avoidable. For amorphous FeN, every Fe atom has four N neighbors and the Fe becomes $Fe^{3+/dipole}$ ideally. The low angular momentum of the $Fe^{3+/dipole}$ and the expanded lattice should take the responsibility for ferro–para magnetic transition upon amorphous FeN formation [2].

The magnetization of a system not only varies with the angular momentum of individual atoms but also their exchange interaction that depends inversely on the atomic separation. These estimations agree with the findings in Refs. [2–6]. For rare earth, the 4f electrons combine less tightly than the 3d electrons of transition metal to their ion cores. Therefore, it is more likely for the 4f electrons to jump to higher energy shells giving the more pronounced increase in M_S as found in Ref. [9]. Apparently, this mechanism accounts for the experimental observations [2–9] more reasonably than the mechanism of N donor effect [4]. It is unlikely for the less electronegative Fe atom to capture electrons from the highly electronegative nitrogen. Therefore, mechanisms of modification on atomic valence, structure order, and atomic separation are complementary and these effects may exist simultaneously determining the magnetic properties of the nitride compounds. However, the valence modification could be dominant in the nitride magnetism.

4.4. Work function reduction for field emission

The work function (Φ) or the threshold (V_T) in cold cathode field emission of materials such as diamond, diamond like carbon (a-C) or carbon nanotubes (CNTs), can be modulated by

Table 2
Variations of angular momentum (unit in μ_B) of Fe with its atomic states

Valence state	Configuration	$S = \sum S_i$	$L = \sum L_i$	$J^a = \sum (L \pm S)_i$
Fe	$3d^6 4s^2$	2	0 (L-frozen)	2 (2.22)
Fe^+	$3d^5 4s^2$	2.5	0	2.5
Fe^{2+}	$3d^5 4s^1$	$2.5 + 0.5$	0	3.0
Fe^{3+}	$3d^4\ 4s^1$	$2.0 + 0.5$	0	2.5
Fe^{4+}	$3d^3 4s^1$	$1.5 + 0.5$	0	2.0
$Fe^{dipole\text{-}1}$	$3d^5 4s^2 4p^1$	$2.5 + 0.5$	$0 + 1$	4.0
$Fe^{dipole\text{-}2}$	$3d^5 4s^2 4d^1$	$2.5 + 0.5$	$0 + 2$	5.0

[a] The total angular momentum is governed by the Hund's rule. $Fe^{dipole\text{-}2}$ corresponds to the antibonding states being well above the E_F.

doping proper amount of properly selected elements besides the geometric enhancement of the emitters. An addition of N to the CVD polycrystalline diamond thin films significantly reduces the V_T of the diamond. The V_T of the N-doped diamond is even lower than the V_T of the diamond doped with boron and phosphorous [10,66–69], as compared in Fig. 10.

Wang et al. [7] deposited carbon nitride films by rf reactive magnetron sputtered carbon in a N_2 discharge. Fig. 11 compares the effect of processing parameters, such as nitrogen partial pressure, substrate temperature, and substrate bias on the field emission properties. The effective work function for deposited carbon nitride films determined using the Fowler–Nordheim equation is in the range of 0.01–0.1 eV at 200 °C substrate temperature under 0.3 Pa nitrogen partial pressure [11]. Li et al. [70] examined the effect of nitrogen-implantation on electron field emission properties of amorphous carbon films. From the Fowler–Nordheim plots, they found that the threshold field is lowered from 14 to 4 V/μm upon increasing the dose of implantation from 0 to 5×10^{17} cm^{-2}. The corresponding effective work function is estimated to be in the range of 0.01–0.10 eV, as illustrated in Fig. 11d. Boron nitride coated graphite nanofibers also emit electrons at much reduced V_T (from 1.5 to 0.8 V/μm) with high (10^2 level) current intensity compared with the uncoated carbon fibers [71]. It is explained that introducing BN nanometric coatings to the surface leads to a significant reduction in the effective potential barrier height, or the Φ. A tendency of N-buckling outward the BN nanotubes has been derived theoretically, which was explained as arising from the different hybridizations of B and N in the curved hexagonal layer and the N-buckling is expected to form a surface dipole [72].

However, understanding the mechanism for the chemically modulated work function of carbon is a great challenge though numerous models have been proposed. The typical models include the negative affinity [73–75], antenna effect of conducting channels [76], impurity gap states [69,77],

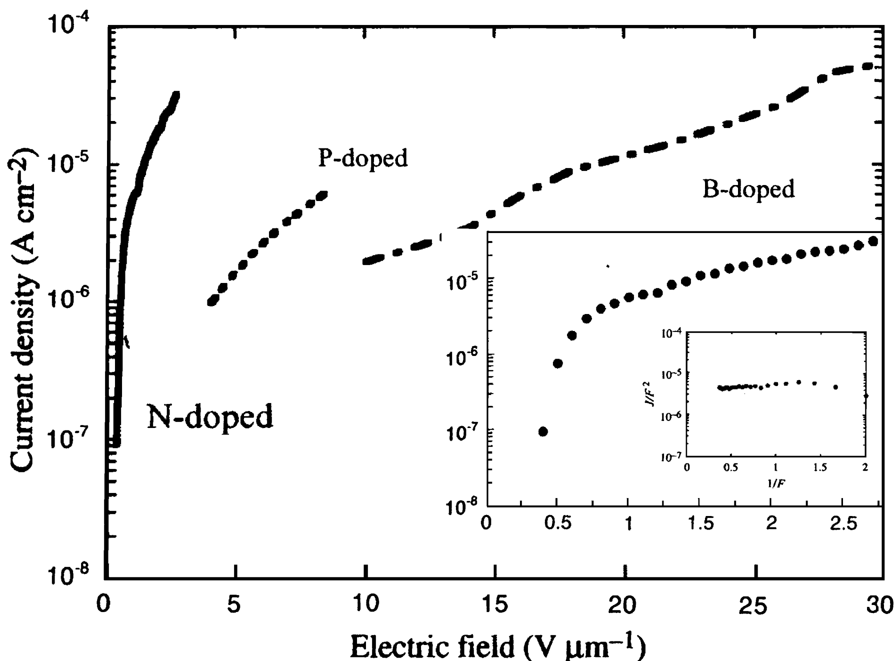

Fig. 10. N, P and B dipping effect on the threshold of cold field electron emission of diamond [10].

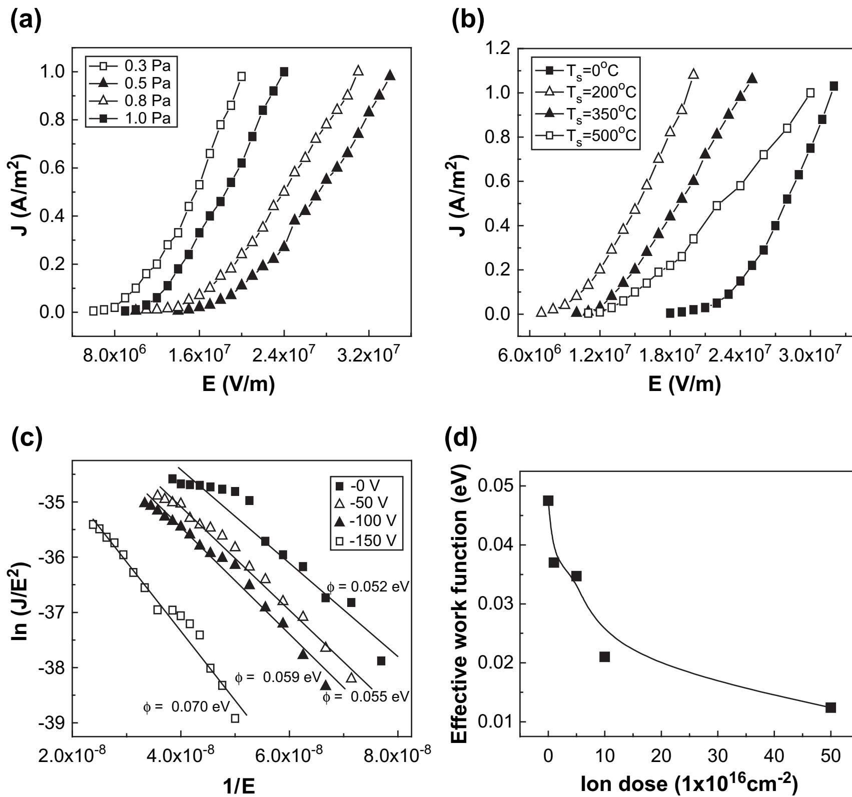

Fig. 11. Filed emission properties of nitrogenated carbon as a function of (a) nitrogen partial pressure, (b) substrate temperature ($P_N = 0.3$ Pa), (c) substrate bias, and (d) N ion implantation dose dependence of effective work function.

band bending at depletion layers [78] and surface dipole formation [79]. The N-lowered V_T has been explained as arising from a certain yet unknown sub-band formed above E_F due to N addition. According to the impurity gap state argument, N locates at a distorted substitutional site in the host matrix with one long but weak C–N bond, which forms a deep singly occupied donor level, ~1.7 eV below the E_C. On the other hand, two neighboring nitrogen atoms relax away from each other due to the weak lone pair interaction, which forms doubly filled states located ~1.5 eV above the E_V. These two mid-gap impurity levels are suggested to play dominant roles in lowering the V_T. Furthermore, N may create a depletion layer that causes band bending at the back contact. At sufficiently high donor concentrations, this band bending narrows the tunneling distance, and allows emission into the diamond conduction band. However, if the N-induced mid-gap impurity levels (1.7 eV $< E_C$ and 1.5 eV $> E_V$) are dominant, the carbon co-doped with P and B should perform better than the carbon doped with N, as the P- and B-derived states (0.46 eV $< E_C$ and 0.38 eV $> E_V$) appear to be more beneficial to the band structure. Boron is a shallow substitutional acceptor in diamond with a level at 0.38 eV above the valence band edge E_V, and phosphorus can act as a shallow donor with a level 0.46 eV below the conduction band edge E_C [80]. Therefore, an atomic scale understanding of the electronic process of threshold reduction due to nitrogenation is highly desirable.

The BBB correlation mechanism could solve the discrepancy regarding the chemical effect on the work function. The weakly bounded 3sp orbitals of a P atom are hard to be hybridized compared with the 2sp orbitals of O and N because the 3sp electrons are more mobile than the 2sp electrons of N and O. The de-localized 3sp electrons determine that the P acts as an n-type donor that adds simply a DOS feature to a position 0.46 eV below the E_C of a diamond [80]. The fact that P-doping gives little reduction of the work function compared to O or N doping [69] means that the impurity gap levels narrow the band gap but contribute little to the work function reduction. Unlike P and B, O and N could expand the band gap of a semiconductor instead, through compound formation. Therefore, N and O act not simply as impurity donors or acceptors in semiconductors, as charge transportation and polarization occurs. The work function of Cs and Li ($\sim$3.5 eV) is much lower than that of other metals ($\sim$5.0 eV). However, adding Cs and Li to the diamond surface is effectless in improving the emission properties. In fact, one is unable to prevent carbide formation in the mixture of metal and carbon. In the process of carbide formation, the conducting electrons of the metal will ‘flow’ from the upper edge of the conduction band to the empty p-orbital of carbon, which lowers the occupied DOS of the doping metals instead. However, doping with both low-Φ metals, such as Li, Cs, and Ga, and electronegative element of N or O could form metal dipoles at the surface, which should reduce the work function of the low-Φ metals even further by $\sim$1.25 eV $<$ 3.5 eV, as discussed. Therefore, co-doping low-Φ metals with O or N could be promising measures [81,82] in lowering the work function of carbon. However, it is anticipated that the production of the H-like bond at the surface due to O or N over-dosing may have detrimental effect on the work function reduction. Appropriate doping would be necessary to avoid H-like bond formation that enlarges the work function [33].

With the BBB correlation as origin, the impurity gap levels (lone pair) [69,77] and the surface dipole formation [79] models would be correct and complete. The lone pair impurities below E_F contribute indirectly to the work function reduction as they induce the antibonding dipoles with the states above E_F. Other effects such as conducting channels [76] and band bending at depletion layers [78] may play some supplementary roles in lowering the V_T, as these effects exist depending less on the presence of oxygen or nitrogen. New understanding may help designing and controlling work function for electron source applications.

4.5. Band-gap expansion for photoemission

The band gap of an intrinsic semiconductor is normally within the infrared range ($E_G \sim 1.0$ eV). After inclusion of N, the band gap is widened significantly as reasoned above. For instance, the band gap of *SiN* increases from 1.1 eV to 3.5 eV with increasing N content [32]. The band-gap enlargement of nitrides has been widely noted. Fig. 12 shows the band-gap enlargement of (a) III nitrides and (b) amorphous Ge- and Si-nitrides. It is noted that nitrogen incorporation into the group-III metallic solids generates a considerably large band gap when the compound is formed. The width of the band gap depends on the bond length [15] or the electronegativity of the corresponding element ($\eta_{Al} = 1.5$, $\eta_{Ga} = 1.6$, and $\eta_{In} = 1.7$). Nitrogen expands the band gap of the semiconductive a-Ge and a-Si from $\sim$1.1 eV to $\sim$4.0 eV [83] depending on nitrogen content. Nitrogen also widens the band gap of amorphous carbon (a-CN_x:H) [84]. Corresponding band-gap changes of a-CN_x:H films have been observed in the He-II valence band spectra showing a recession of the leading edge of more than 0.9 eV while the optical band gap widens from 0 eV to 1 eV or more.

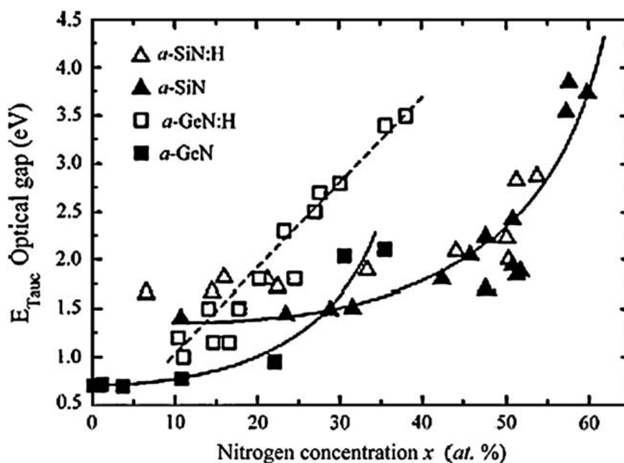

Fig. 12. (a) N concentration dependence of the optical band gap (E_{Tauc}) of a-Ge:N:H [87,88] and a-Si:N:H [89] thin films.

Reynolds et al. [14] suggested that the green-band of ZnO and the yellow-band of GaN share some common yet unclear mechanisms. Chambouleyron and Zanatta [83] related the band-gap expansion of a-Ge:N and a-Si:N compounds to the substitution of Si–Si or Ge–Ge bonds by stronger Si–N or Ge–N bonds. It was suggested that, as the N content increases, the nitrogen lone pair band develops and that the lone pair band dominates the valence band maximum as the stoichiometry is reached. The largest optical band gap is obtained for the stoichiometric compound. On the contrary, for smaller N content, Si–Si or Ge–Ge bonds dominate the valence band maximum.

For amorphous semiconductors, it is generally accepted that the transition of carriers is between the conduction band and the valence band tail states. Luminescence spectra [32] of the a-Si:H showed that the n-type (phosphorous) doping shifts the luminescence peak of the a-Si:H from 1.1 eV to 0.81 eV, and the p-type (boron) doping shifts the peak from 1.1 to 0.91 eV. This can be easily understood in terms of impurity levels. The shallow n-donor levels and the deeper p-acceptor levels are located within the initial band gap (1.1 eV width) near to the band tails, which should narrow the gap, as observed. However, the luminescence peak of the a-Si:N:H compound moves to higher energy with increasing nitrogen concentration [85]. The broadened band gap through nitridation could not be explained in terms of the traditional donor effect, though the nitrogen addition is always believed as n-type doping. Clearly, the band gaps of metal nitride, III-nitride, and IV-nitride are enlarged by the same hole-production mechanism proposed in the BBB correlation premise. The change in bond nature and bond length has an effect on the crystal field, and consequently, the width of the band gap; charge transport in the reaction re-populates with valence electrons of the host materials. The band-gap expansion mechanism may also explain the increase in resistivity and activation energy of the CN films with nitrogen incorporation [86] because of the transition from metallic to semiconducting behavior.

5. Summary

Consistent understanding of the unusual performance of a nitride has been developed from the perspective of bond–band–barrier correlation. It is clear that the N-enhanced magnetization, the blue shift in nitride light emission, the N-lowered threshold of cold cathode in carbon,

wear and corrosion resistance and super elastic nitrides all arise from the nitride tetrahedron bond formation with the involvement of bonding, nonbonding, hole and antibond dipole production. Therefore, the extent and type of nitrogen lone pair interactions are the most important functional groups present not only in the organic molecules [90] but also in inorganic compounds. A combination of density functional calculation and UPS measurement would be most effective in revealing the dynamics of bond and band formation. Besides, the current BBB correlation model could provide complementary mechanism to correlate the electronic configuration in the bonding process and its derivatives on the valence *DOS* and physical properties. Further extension of the BBB correlation and the concept of lone pair nonbonding, antibonding dipoles and hole states may provide guidelines for controllable modification of existing materials and in the pursuit of new functional properties. The current interpretation may be helpful in thinking about the nitride in a bond forming way, which can be considered in calculation refinement. This will stimulate more topics of research, such as quantification of the bond geometry and determination of bonding energy for specific systems, towards controlling bond-and-band forming and hence designer processes and materials.

Note: We are aware while proofing the first-principle calculations by Zhang, Sun, and Chen[1] suggested that the strength of the previously predicted hardest C_3N_4 phase is lower compared to not only diamond but also cubic boron nitride by a surprisingly large amount. They indicated that the excessive electrons on the N atoms play a key role in determining the high elasticity and low hardness, which concurs with the current BBB prediction.

Acknowledgment

Helpful discussions with Professors Stan Veprek, Chunli Bai, John S. Colligon, S.R.P. Silva, David S.Y. Tong, F.M. Ashby, Wei Gao, Philip J. Jennings, Xi Yao, A. Bhalla, E. Sacher, and En-Yong Jiang, and editorial advice given by Mas Subramanian are all gratefully acknowledged. WTZ acknowledges funding support from the Teaching and Research Award Program for OYTHEI of MOE, NFSC under Grant No. 50525204 and the special foundation for PhD program in High Education Institutes, P.R.C., from Ministry of Chinese Education and the Tan Chin Tuan Fellowship at Nanyang Technological University, Singapore. Permission for reprinting diagrams from Elsevier Science, IOP, APS, and AIP is also acknowledged.

References

[1] Schaaf P. Prog Mater Sci 2002;47:1.
[2] Jack KH. Proc R Soc (London) 1951;A208:216–24.
[3] Jack KH. Mater Sci Forum 2000;325–326:91.
[4] Jiang EY, Sun CQ, Liu Y, Li J. J Appl Phys 1989;65:1659.
[5] Jiang EY, Sun DC, Lin C, Tian MB, Bai HL, Ming SL. J Appl Phys 1995;78:2596.
[6] Sun DC, Lin C, Jiang EY. J Phys Condens Matter 1995;7:3667.
[7] Wang X, Zheng WT, Tian HW, Yu SS, Xu W, Meng SH, et al. Appl Surf Sci 2003;220:30.
[8] Coey JMD, Sun H. J Magn Magn Mater 1990;87:L251.
[9] Pan H, Yang F, Chen Y, Han X, Tang N, Chen P, et al. J Phys Condens Matter 1997;9:2499.

[1] Zhang Y, Sun H, and Chen CF, Phys Rev B 2006;73:064109.

[10] Okano K, Koizumi S, Silva SRP, Amaratunga GAJ. Nature 1996;381:140.
[11] Zheng WT, Li JJ, Wang X, Li XT, Jin ZS, Tay BK, et al. J Appl Phys 2003;94:2741.
[12] Agrawal BK, Agrawal S, Yadov PS, Kumar S. J Phys Condens Matter 1997;9:1763.
[13] Yang Z, Xu Z. J Phys 1996;C8:8303.
[14] Reynolds DC, Look DC, Jogai B, Morkoc H. Solid State Commun 1997;101:643.
[15] Ponce FA, Bour DP. Nature 1997;386:351.
[16] Cahn RW. Nature 1996;380:104.
[17] Guo YJ, Goddard WA. Chem Phys Lett 1995;237:72.
[18] Badding JV, Nesting DC. Chem Mater 1996;8:1535.
[19] Hughbanks T, Tian T. Solid State Commun 1995;96:321.
[20] Teter DM, Hemley RJ. Science 1996;271:53.
[21] Niu C, Lu YZ, Lieber CM. Science 1993;261:334.
[22] Leiber CM, Zhang Z. J Adv Mater 1994;6:497.
[23] Sjonstrom H, Stafstrom S, Boman M, Sundgren JE. Phys Rev Lett 1995;75:1336.
[24] Amaratunga GAJ, Chhowalla M, Kiely CJ, Alexandrou I, Aharonov R, Devenish RM. Nature 1996;383:321.
[25] Sun CQ, Tay BK, Lau SP, Sun XW, Zeng XT, Bai HL, et al. J Appl Phys 2001;90:2615.
[26] Zheng WT, Sjostrom H, Ivanov I, Xing KZ, Broitman E, Salaneck WR, et al. J Vac Sci Technol 1996;A14:2696.
[27] Broitman E, Zheng WT, Sjostrom H, Ivanov I, Greene JE, Sundgreen JE. Appl Phys Lett 1998;72:2532.
[28] Caceres D, Vergara I, Gonzalez R, Monroy E, Calle F, Munoz E, et al. J Appl Phys 1999;86:6773.
[29] Sun CQ. Appl Phys Lett 1998;72:1706.
[30] Sun CQ. Prog Mater Sci 2003;48:521.
[31] Atkins PW. Physical chemistry. 4th ed. Oxford University Press; 1990. p. P409, P646.
[32] Street RA. Hydrogenated amorphous silicon. Cambridge University Press; 1991. p. 276, 315, 295.
[33] Zheng WT, Tay BK, Sun CQ. Solid State Commun 2003;128:385.
[34] Fu YQ, Sun CQ, Du HJ, Yan BB. J Phys D 2001;34:1430.
[35] Sotto M, Gaushier S, Pourmir F, Rousset S, Klein J. Surf Sci 1997;371:36.
[36] Schwegmann S, Seitsonen AP, Dietrich H, Bludau H, Over H, Jacobi K, et al. Chem Phys Lett 1997;264:680.
[37] Bermudez VM. Surf Sci 2002;499:124.
[38] Sun CQ. Surf Rev Lett 2000;7:347.
[39] Stolbov S, Hong S, Kara A, Rahman TS. Phys Rev B 2005;72:155423.
[40] Sun CQ, Fu YQ, Yan BB, Hsieh JH, Lau SP, Sun XW, et al. J Appl Phys 2002;91:2051.
[41] Driss-Khodja M, Gheorghiu A, Dufour G, Roulet H, Senemaud C, Cauchetier M. Phys Rev 1996;B53:4287.
[42] Schwegmann S, Seitsonen AP, De Renzi V, Dietrich H, Bludau H, Gierer M, et al. Phys Rev B 1998;57:15487.
[43] Terrones M, Ajayan PM, Banhart F, Blase X, Carroll DL, Charlier JC, et al. Appl Phys A 2002;74:355.
[44] Hellgren N, Guo JH, Luo Y, Sathe C, Agui A, Kashtanov S. Thin Solid Films 2005;471:19.
[45] Davydov VY, Emtsev VV, Goncharuk IN, Smirnov AN, Petrikov VD, Mamutin VV, et al. Appl Phys Lett 1999;75:3297.
[46] Han WG, Zhang CT. J Phys Condens Matter 1991;3:27.
[47] Fanchini G, Tagliaferro A, Ray SC. Diamond Relat Mater 2003;12:208.
[48] Fanchini G, Tagliaferro A, Conway NMJ, Godet C. Phys Rev 2003;B66:195415.
[49] Tibbetts GG, Burkstrand JM, Tracy JC. Phys Rev B 1977;15:3652.
[50] Fuentes GG, Elizalde E, Sanz JM. J Appl Phys 2001;90:2737.
[51] Souto S, Pickholz M, Dos Santos MC, Alvarez F. Phys Rev B 1998;57:2536.
[52] Chen ZY, Zhao JP, Yano T, Ooie T. J Appl Phys 2002;92:281.
[53] Tibbetts GG, Burkstrand JM. Phys Rev B 1977;16:1536.
[54] Veprek S. J Vac Sci Technol 1999;A17:2401.
[55] Wang EG. Prog Mater Sci 1997;41:241.
[56] Malkow T. Mater Sci Eng 2000;A292:112.
[57] Lv Q, Cao CB, Li C, Zhang JT, Zhu HX, Kong X, et al. J Mater Chem 2003;13:1241.
[58] Veprek S. Thin Solid Films 1997;297:145.
[59] Veprek S. Thin Solid Films 1995;268:64.
[60] Pan Z, Sun Z, Xie Z, Hao L, Wei S, Xu J, et al. <http://www.paper.edu.cn/200511-444>.
[61] Zeng XT. Surf Coat Technol 1999;113:75.
[62] Zeng XT, Zhang S, Sun CQ, Liu YC. Thin Solid Films 2003;424:99.
[63] Zhou JP, Li D, Gu YS, Chang XR, Zhao CH, Li FH, et al. Sci China Ser A 2002;45:255.
[64] Zhong WH, Tay BK, Lau SP, Sun XW, Li S, Sun CQ. Thin Solid Films 2005;478:61.

[65] Sun CQ, Zhong WH, Li S, Tay BK. J Phys Chem B 2004;108:1080.
[66] Cheah LK, Shi X, Liu E, Tay BK. J Appl Phys 1999;85:6816.
[67] Lim SC, Stallcup II RE, Akwani IA, Perez JM. Appl Phys Lett 1999;75:1179.
[68] Sowers AT, Ward BL, English SL, Nemanich RJ. J Appl Phys 1999;86:3973.
[69] Robertson J. J Vac Sci Technol B 1999;17:659.
[70] Li JJ, Zheng WT, Gu CZ, Jin ZS, Zhao YN, Mei XX, et al. Carbon 2004;42:2309.
[71] Sugino T, Yamamoto T, Kimura C, Murakami H, Hirakawa M. Appl Phys Lett 2002;80:3808.
[72] Hernández E, Goze C, Bernier P, Rubio A. Phys Rev Lett 1998;80:4502.
[73] Zhu W, Kochanski GP, Jin S. Science 1998;282:1471.
[74] Geis MW, Efremow NN, Krohn KE, Twitchell JC, Lyszczarz TM, Kalish R, et al. Nature (London) 1998;393:31.
[75] Bandis C, Pate B. Appl Phys Lett 1996;69:366.
[76] Xu WS, Tzeng T, Latham RV. J Phys D 1993;26:1776.
[77] Rutter MJ, Robertson J. Phys Rev B 1998;57:9241.
[78] Amaratunga GAJ, Silva SRP. Appl Phys Lett 1996;68:2529.
[79] Zhao JP, Chen ZY, Wang X, Shi TS. J Non-Cryst Solids 2001;291:181.
[80] Briddon P, Jones R. Phys B Condens Matter 1993;185:179.
[81] Pickett WE. Phys Rev Lett 1994;73:1664.
[82] Lin LW. J Vac Sci Technol A 1998;6:1053.
[83] Chambouleyron I, Zanatta AR. J Appl Phys 1998;84:1.
[84] Hammer P, Victoria NM, Alvarez F. J Vac Sci Technol A 1998;16:2941.
[85] Austin IG, Jackson WA, Searle TM, Bhat PK, Gibson RA. Philos Mag B 1985;52:271.
[86] Monclus MA, Cameron DC, Chowdhury AKMS, Barkley R, Collins M. Thin Solid Films 1999;356:79.
[87] Zanatta AR, Chambouleyron I. Phys Rev B 1993;48:4560.
[88] Vilcarromero J, Marques FC. Phys Status Solidi B 1995;192:543.
[89] Hasegawa S, Matsuda M, Kurata Y. Appl Phys Lett 1991;58:741.
[90] Novak I, Kovac B, Klasinc L, Ostrovski VA. Spectrochim Acta Part A 2003;59(8):1725.